Received December 2001
Revised July 2002
Accepted August 2002

Numerical simulation of heat transfer of turbulent impinging jets with two-equation turbulence models

Bart Merci, Jan Vierendeels, Chris De Langhe and Erik Dick
Department of Flow, Heat and Combustion Mechanics, Gent University, Gent, Belgium

Keywords *Heat transfer, Impinging jets, Numerical analysis*

Abstract *A numerical scheme that has already proved to be efficient and accurate for laminar heat transfer is extended for turbulent, axisymmetric heat transfer calculations. The extended scheme is applied to the steady-state heat transfer of axisymmetric turbulent jets, impinging onto a flat plate. Firstly, the low-Reynolds version of the standard k-ε model is employed. As is well known, the classical k-ε turbulence model fails to predict the heat transfer of impinging jets adequately. A non-linear k-ε model, with improved ε-equation, yields much better results. The numerical treatment of the higher order terms in this model is described. The effect on the heat transfer predictions of a variable turbulent Prandtl number is shown to be small. It is also verified that the energy equation can be simplified, without affecting the results. Results are presented for the flow field and the local Nusselt number profiles on the plate for impinging jets with different distances between the pipe exit and the flat plate.*

1. Introduction

Heat transfer by turbulent impinging jets is important for many engineering applications. Often, the local heat transfer or the local value of the Nusselt number, has to be known. Numerical simulations should be able to yield reliable predictions. However, as Behnia *et al.* (1998, 1999) illustrated, the standard k-xε model, in combination with a constant turbulent Prandtl number (Pr_t), does not yield accurate results.

Extensive research has already been done on this subject. Within the class of eddy viscosity turbulence models, two types of models perform well. Firstly, there is the v^2-f model by Durbin (1991). This model produces very good results for impinging flows, in particular for heat transfer predictions (Behnia *et al.*, 1998, 1999). Results are presented in those references for both constant and variable Pr_t: the influence of a variable Prandtl number is small. The price for the accurate results is the solution of an additional transport equation (for v^2) and an elliptic equation for the relaxation factor f. Therefore, this model is more time consuming than non-linear two-equation eddy viscosity turbulence models. In such models, the linear relation between the turbulent stresses and the local strain rate tensor (as in the standard k-ε model and the v^2-f model)

International Journal of Numerical Methods for Heat & Fluid Flow
Vol. 13 No. 1, 2003
pp. 110-132

0961-5539
DOI 10.1108/09615530310456787

is replaced by a non-linear relation between the turbulent stresses and the local strain rate and vorticity tensors. The second well performing model belongs to this class: the most recent formulation of Craft *et al.* (2000) model, yields very good heat transfer predictions for impinging jets onto a flat plate. The transport equation for the dissipation rate ε is modified with the "Yap" correction (Yap, 1987). A constant Pr_t is used. However, the relation between the turbulent stresses and the local mean velocity gradients contains a term which is physically inconsistent with respect to certain realizable conditions (Speziale, 1998). In this paper, a non-linear eddy-viscosity model is presented which does not violate these conditions.

Both in Behnia *et al.* (1998, 1999) and Craft *et al.* (2000), the work done by viscous and turbulent stresses are neglected in the energy equation, as well as the contributions from the kinetic energy (both mean and turbulent) in the total enthalpy. In this paper, this is justified.

The purpose of this paper is not only suggesting a new turbulence model, but also applying an accurate numerical method to the heat transfer in a turbulent axisymmetric jet, impinging onto a flat plate. Firstly, the implemented numerical method is described. It is presented as an extension of the method, developed for laminar two-dimensional flows (Vierendeels *et al.* , 1999, 2001). The numerical treatment of the higher order terms in the non-linear eddy-viscosity model is described. Next, the accuracy of the scheme is illustrated by application to the mentioned flow. The overprediction of the Nusselt number on the axis by the standard k-ε model with a constant Pr_t, is well reproduced. Next, it is illustrated that it is justified to neglect the mentioned terms in the energy equation. Finally, the presented non-linear eddy-viscosity model is shown to yield better results than (a low-Reynolds version of) the standard k-ε model, both in terms of the Nusselt number at the stagnation point and the shape of the local Nusselt number profile along the plate. Also the flow field predictions are in better agreement with experimental data.

2. Numerical scheme

2.1 Governing equations

The steady-state transport in vector integral formulation for a control volume V with boundary S, are:

$$\begin{cases} \oint_S \rho\bar{v}\cdot\bar{n}\mathrm{d}S = 0 \\ \oint_S \rho\bar{v}(\bar{v}\cdot\bar{n})\mathrm{d}S + \oint_S p_{\mathrm{eff}}\bar{n}\mathrm{d}S = \oint_S \bar{\bar{\tau}}\bar{n}\mathrm{d}S \\ \oint_S \rho H\bar{v}\cdot\bar{n}\mathrm{d}S = \oint_S [\bar{\bar{\tau}}\bar{v}]\cdot\bar{n}\mathrm{d}S + \oint_S \bar{q}\cdot\bar{n}\mathrm{d}S \\ \oint_S \rho k\bar{v}\cdot\bar{n}\mathrm{d}S = \oint_S \left(\mu + \frac{\mu_t}{\sigma_k}\right)(\nabla k)\cdot\bar{n}\mathrm{d}S + \int_V S_k \mathrm{d}V \\ \oint_S \rho\varepsilon\bar{v}\cdot\bar{n}\mathrm{d}S = \oint_S \left(\mu + \frac{\mu_t}{\sigma_\varepsilon}\right)(\nabla\varepsilon)\cdot\bar{n}\mathrm{d}S + \int_V S_\varepsilon \mathrm{d}V \end{cases} \quad (1)$$

Note that in equation (1) external forces (such as gravity) and internal heat sources are absent. Equation (1) is Favre averaged Navier-Stokes equations, but all averaging symbols are omitted. Favre averaging is used, since the density ρ is a variable. In equation (1), $\bar{v}$ is the velocity vector and $\bar{n}$ the outward normal on the surface S. The "effective" pressure p_{eff} is defined as:

$$p_{\text{eff}} = p + \tfrac{2}{3}\rho k, \tag{2}$$

where

$$k = \tfrac{1}{2} v_i'' \tilde{v}_i''$$

is the turbulence kinetic energy (v_i'' is the Favre fluctuation of velocity component v_i). The stress tensor:

$$\bar{\bar{\tau}} = \bar{\bar{\tau}}^m + \bar{\bar{\tau}}^t - \tfrac{2}{3}\rho k \bar{\bar{I}}, \tag{3}$$

consists of a molecular and a turbulent part. The molecular tensor is:

$$\tau_{ij}^m = 2\mu S_{ij}, \tag{4}$$

where μ is the molecular viscosity and S_{ij} the strain rate tensor:

$$S_{ij} = \frac{1}{2}\left(\frac{\partial v_i}{\partial x_j} + \frac{\partial v_j}{\partial x_i}\right) - \frac{1}{3}\delta_{ij}\frac{\partial v_k}{\partial x_k}, \tag{5}$$

with δ_{ij} the Kronecker delta. The turbulent stress tensor $\bar{\bar{\tau}}^t$ is defined as:

$$\tau_{ij}^t - \delta_{ij}\tfrac{2}{3}\rho k = \tau_{ij}^{(1)} + \tau_{ij}^{(2)}, \tag{6}$$

where $\bar{\bar{\tau}}^{(1)}$ is the first order part, defined as:

$$\tau_{ij}^{(1)} = 2\mu_t S_{ij}, \tag{7}$$

with μ_t the eddy viscosity. Details on the definition of μ_t and the second order part are discussed in Section 3. Note that the last term in equation (3) (with $\bar{\bar{I}}$ the unity tensor) has been added since the contribution of $^2/_3\,\rho k$ is accounted for in the effective pressure (equation (2)).

The total enthalpy H is given by:

$$H = e + \frac{v^2}{2} + k + \frac{p_{\text{eff}}}{\rho}, \tag{8}$$

where e stands for the internal energy and v^2 is the velocity magnitude squared.

The heat flux $\bar{q}$ consists of a molecular and a turbulent part:

$$\bar{q} = -\lambda \nabla T - \frac{\mu_t c_p}{\mathrm{Pr_t}} \nabla T, \tag{9}$$

where λ is the heat conduction coefficient, T the temperature, c_p the specific heat at constant pressure. Note that the linear gradient hypothesis is used for the turbulent heat flux. This is also done for the diffusion terms of the turbulent kinetic energy k and the dissipation rate ε. Finally, S_k and S_ε are source terms for k and ε. It is noteworthy that the energy equation is written in its most complete form. In the discussion of the results, it will be verified that a reduced form can be used without loss of accuracy.

2.2 Discretization and solution procedure

Details on the discretization and time marching method for two-dimensional laminar flows, are found elsewhere (Vierendeels *et al.*, 1999, 2001). Here, the extension towards turbulent axisymmetric flows is described.

2.2.1 Spatial discretization. The steady-state equations (1) are discretized on a wedge-like control volume with angle Θ (Figure 1). For simplicity, the cells are rectangular in a plane that contains the symmetry axis. A vertex-centred finite volume method is applied. Some geometrical quantities are defined first:

$$x_{i\pm1/2} = \tfrac{1}{2}(x_i + x_{i\pm1}); \;\; y_{j\pm1/2} = \tfrac{1}{2}(y_j + y_{j\pm1}); \tag{10}$$

$$\Delta x_i = x_{i+1/2} - x_{i-1/2}; \;\; \Delta y_j = y_{j+1/2} - y_{j-1/2}. \tag{11}$$

The spatially discretized form of equation (1) becomes (after division by Θ):

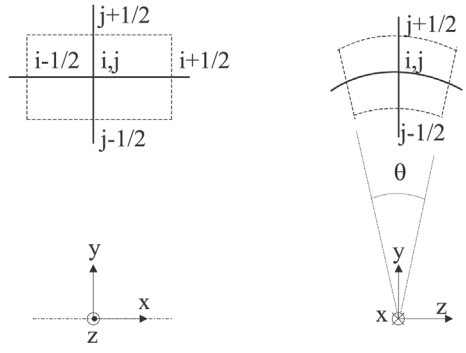

Figure 1.
Axisymmetric vertex-centred control volume

$$
\begin{aligned}
&[(F_c + F_a)_{i+1/2} - (F_c + F_a)_{i-1/2}]y_j\Delta y_j + [(G_c + G_a)_{j+1/2}y_{j+1/2} \\
&\quad - (G_c + G_a)_{j-1/2}y_{j-1/2}]\Delta x_i + A_{a,i,j}\Delta x_i\Delta y_j = (F^{(1)}_{v,i+1/2} - F^{(1)}_{v,i-1/2})y_j\Delta y_j \\
&\quad + (F^{(2)}_{v,i+1/2} - F^{(2)}_{v,i-1/2})y_j\Delta y_j + (G^{(1)}_{v,j+1/2}y_{j+1/2} \\
&\quad - G^{(1)}_{v,j-1/2}y_{j-1/2})\Delta x_i + (G^{(2)}_{v,j+1/2}y_{j+1/2} \\
&\quad - G^{(2)}_{v,j-1/2}y_{j-1/2})\Delta x_i + A_{v,i,j}\Delta x_i\Delta y_j + S_{i,j}y_j\Delta x_i\Delta y_j
\end{aligned} \tag{12}
$$

The different fluxes in equation (12) are:

$$F_{c,i\pm1/2} = u_{i\pm1/2}[0 \;\; \rho u \;\; \rho v \;\; 0 \;\; \rho k \;\; \rho\varepsilon]^T_{L/R} \tag{13}$$

$$G_{c,j\pm1/2} = v_{j\pm1/2}[0 \;\; \rho u \;\; \rho v \;\; 0 \;\; \rho k \;\; \rho\varepsilon]^T_{L/R} \tag{14}$$

$$F_{a,i\pm1/2} = [\rho u \;\; p_{\text{eff}} \;\; 0 \;\; \rho H u \;\; 0 \;\; 0]^T_{i\pm1/2} \tag{15}$$

$$G_{a,j\pm1/2} = [\rho v \;\; 0 \;\; p_{\text{eff}} \;\; \rho H v \;\; 0 \;\; 0]^T_{j\pm1/2} \tag{16}$$

$$A_{a,i,j} = [0 \;\; 0 \;\; -p_{\text{eff}} \;\; 0 \;\; 0 \;\; 0]^T_{i,j} \tag{17}$$

$$F^{(1)}_{v,i\pm1/2} = \left[0 \;\; \tau_{xx} \;\; \tau^m_{xy} + \tau^{(1)}_{xy} \;\; u\tau_{xx} + v\tau_{xy} + q_x \;\; \mu_{\text{eff},k}\frac{\partial k}{\partial x} \;\; \mu_{\text{eff},\varepsilon}\frac{\partial \varepsilon}{\partial x}\right]^T_{i\pm1/2} \tag{18}$$

$$G^{(1)}_{v,j\pm1/2} = \left[0 \;\; \tau^m_{yx} + \tau^{(1)}_{yx} \;\; \tau_{yy} \;\; u\tau_{yx} + v\tau_{yy} + q_y \;\; \mu_{\text{eff},k}\frac{\partial k}{\partial y} \;\; \mu_{\text{eff},\varepsilon}\frac{\partial \varepsilon}{\partial y}\right]^T_{j\pm1/2} \tag{19}$$

$$F^{(2)}_{v,i\pm1/2} = [0 \;\; 0 \;\; \tau^{(2)}_{xy} \;\; 0 \;\; 0 \;\; 0]^T_{i\pm1/2} \tag{20}$$

$$G^{(2)}_{v,j\pm1/2} = [0 \;\; \tau^{(2)}_{yx} \;\; 0 \;\; 0 \;\; 0 \;\; 0]^T_{j\pm1/2} \tag{21}$$

$$A_{v,i,j} = [0 \;\; 0 \;\; -\tau_{zz} \;\; 0 \;\; 0 \;\; 0]^T_{i,j} \tag{22}$$

$$S_{i,j} = [0 \;\; 0 \;\; 0 \;\; 0 \;\; S_k \;\; S_\varepsilon]^T_{i,j}, \tag{23}$$

where T denotes the transpose of the matrix, c stands for convective, a for acoustic and v for viscous. The contributions A_a and A_v are a consequence of axisymmetry. The tensor component τ_{zz} is written in terms of the radial velocity through the relation $\frac{\partial w}{\partial z} = \frac{v}{y}$.

In the convective fluxes, velocity upwinding is applied, with the L/R (left/right) values extrapolated with the van Leer-κ method (van Leer, 1977), with $\kappa = {}^1/_3$. Consequently, third order accuracy is obtained on a Cartesian grid. The acoustic and viscous terms are discretized centrally. The sources $S_{i,j}$ and the "axisymmetric contributions" $A_{a,i,j}$ and $A_{v,i,j}$ are evaluated nodewise. Artificial dissipation terms for pressure and temperature are added to the mass flux in x-direction (at cell face $i + {}^1/_2$):

$$F_{d,i+1/2} = \frac{1}{2}\left[\frac{p_{\text{eff},i} - p_{\text{eff},i+1}}{\beta_x} + |u|_{i+1/2}\rho_T(T_i - T_{i+1})\right], \tag{24}$$

and similar additions are done at cell face $i - {}^1/_2$ and in the y-direction. In equation (24), ρ_T stands for the partial derivative of ρ with respect to T, and $\beta_{x/y}$ is given by:

$$\beta_{x/y} = w_r + \frac{2(\mu + \mu_t)}{\rho\Delta(x/y)}, \tag{25}$$

where $w_r = \sqrt{u^2 + v^2}$ is the local velocity.

2.2.2 Time marching method. The steady state solution of equation (12) is obtained by stepping in pseudo-time:

$$\Gamma\frac{\partial Q}{\partial \tau}y_j \;\Delta x_i \Delta y_j + C_c + C_a = C_v + C_S. \tag{26}$$

In equation (26), C_c denotes the contribution of the convective terms, C_a the acoustic terms, C_v the viscous terms and C_S the sources. The vector Q consists of the primitive variables:

$$Q = [\,p_{\text{eff}} \;\; u \;\; v \;\; T \;\; k \;\; \varepsilon]^T. \tag{27}$$

The complete set of equation (12) is decoupled into two subsets: the RANS equations on the one hand, and the transport equations for the turbulence quantities on the other hand.

For the RANS subset, preconditioning is applied. A simplified form of the precondtioner (Weiss and Smith, 1995) is used, suitable for low-Mach turbulent flows (Vierendeels *et al.*, 1999):

$$\Gamma_{\mathrm{RANS}} = \begin{bmatrix} \alpha & 0 & 0 & \rho_T \\ 0 & \rho & 0 & 0 \\ 0 & 0 & \rho & 0 \\ \alpha H - 1 & 0 & 0 & 0 \end{bmatrix}, \tag{28}$$

where

$$\alpha = \frac{1}{\beta^2} - \frac{\rho_T}{\rho c_p}.$$

Herein is $\beta = \beta_x$ for lines in the y-direction and $\beta = \beta_y$ for lines in the x-direction (with $\beta_{x/y}$ from equation (25)). For the turbulence equations, there is no preconditioning ($\Gamma_{\mathrm{turb}} = \mathrm{diag}(\rho, \rho)$).

The time stepping is done through a multistage scheme with four stages. The value at pseudo-time level $(n+1)$ is obtained by:

$$\begin{aligned} Q^{(0)} &= Q^n \\ Q^{(m+1)} &= Q^n + \alpha_{m+1} cfl \Delta Q^{(m)} \quad , m = 0, \ldots, 3 \\ Q^{n+1} &= Q^{(4)}, \end{aligned} \tag{29}$$

with $(\alpha_1, \alpha_2, \alpha_3, \alpha_4)$ equal to $(^1/_4, ^1/_3, ^1/_2, 1)$ and $cfl = 1$. For each stage, $\Delta Q^{(m)} = Q^{(m+1)^*} - Q^{(m)}$ is calculated as (for lines in the y-direction):

$$\begin{aligned} &\left(\frac{\Gamma}{\Delta\tau} y_j \, \Delta x_i \Delta y_j + \mathrm{M_v} + \mathrm{M_d}\right)(Q^{(m+1)^*} - Q^{(m)}) \\ &+ [(F_{\mathrm{c}}^{(m)} + F_{\mathrm{a}}^{(m)} + F_{\mathrm{d}}^{(m)})_{i+1/2} - (F_{\mathrm{c}}^{(m)} + F_{\mathrm{a}}^{(m)} + F_{\mathrm{d}}^{(m)})_{i-1/2}] y_j \Delta y_j + (G_{\mathrm{c}}^{(m)} \\ &+ G_{\mathrm{a}}^{(m+1)^*} + G_{\mathrm{d}}^{(m+1)^*})_{j+1/2} \, y_{j+1/2} \, \Delta x_i \\ &- (G_{\mathrm{c}}^{(m)} + G_{\mathrm{a}}^{(m+1)^*} + G_{\mathrm{d}}^{(m+1)^*})_{j-1/2} \, y_{j-1/2} \, \Delta x_i + A_{\mathrm{a},i,j}^{(m+1)^*} \Delta x_i \Delta y_j \\ &= (F_{\mathrm{v},i+1/2}^{(1)^{(m)}} - F_{\mathrm{v},i-1/2}^{(1)^{(m)}}) y_j \Delta y_j + (F_{\mathrm{v},i+1/2}^{(2)^{(m)}} - F_{\mathrm{v},i-1/2}^{(2)^{(m)}}) y_j \Delta y_j \\ &+ G_{\mathrm{v},j+1/2}^{(1)^{(m+1)^*}} \, y_{j+1/2} \Delta x_i - G_{\mathrm{v},j-1/2}^{(1)^{(m+1)^*}} \, y_{j-1/2} \Delta x_i \\ &+ G_{\mathrm{v},j+1/2}^{(2)^{(m)}} \, y_{j+1/2} \Delta x_i - G_{\mathrm{v},j-1/2}^{(2)^{(m)^*}} \, y_{j-1/2} \Delta x_i \\ &+ A_{\mathrm{v},i,j}^{(m+1)^*} \Delta x_i \Delta y_j + S_{i,j}^{(m),(m+1)^*} \, y_j \Delta x_i \Delta y_j. \end{aligned} \tag{30}$$

Note that, in comparison to equation (12), the artificial dissipation terms (equation (24)) have been added. They are only non-zero for the RANS subset. There, the matrices M_v and M_d account for the contribution on the implicitly treated line (in y-direction) of the viscous and artificial dissipation fluxes in the x-direction:

$$M_v = y_j \Delta y_j \left(\frac{R_{xx,i-1/2}}{\Delta x_{i-1/2}} + \frac{R_{xx,i+1/2}}{\Delta x_{i+1/2}} \right), \tag{31}$$

with R_{xx} given by:

$$R_{xx} = \begin{bmatrix} 0 & 0 & 0 & 0 \\ 0 & \frac{4}{3}(\mu + \mu_t) & 0 & 0 \\ 0 & 0 & \mu + \mu_t & 0 \\ 0 & \frac{4}{3}(\mu + \mu_t)u & (\mu + \mu_t)v & \lambda + \frac{\mu_t c_p}{\mathrm{Pr_t}} \end{bmatrix} \tag{32}$$

and:

$$M_d = y_j \ \Delta y_j (D_{xx,i-1/2} + D_{xx,i+1/2}), \tag{33}$$

with D_{xx} defined as:

$$D_{xx} = \begin{bmatrix} \frac{1}{2\beta_x} & 0 & 0 & \frac{1}{2}|u|\rho_T \\ \frac{u}{2\beta_x} & 0 & 0 & \frac{1}{2}|u|\rho_T u \\ \frac{v}{2\beta_x} & 0 & 0 & \frac{1}{2}|u|\rho_T v \\ \frac{H}{2\beta_x} & 0 & 0 & \frac{1}{2}|u|\rho_T H \end{bmatrix}. \tag{34}$$

Similar expressions are used for lines in the x-direction. The superscripts (m),$(m+1)^*$ for the sources denote that they are partly treated explicitly and partly implicitly, which is important for the turbulence transport equations.

The treatment of the different terms of the turbulent stress tensor (equation (6)) in the discretization (equation (30)) is explained in Section (2.3).

The acoustic flux on level $(m+1)^*$ is defined as:

$$G_a^{(m+1)^*} = \begin{bmatrix} \rho^{(m)} v^{(m+1)^*} \\ 0 \\ p_{\mathrm{eff}}^{(m+1)^*} \\ \rho^{(m)} H^{(m)} v^{(m+1)^*} \end{bmatrix}. \tag{35}$$

The pseudo-time step for lines in the y-direction is calculated as:

$$\Delta\tau = \left(\frac{|u| + c_x}{\Delta x} + \frac{2|v|}{\Delta y}\right)^{-1}, \tag{36}$$

as described in Vierendeels (1999). Here $c_x = \sqrt{u^2 + \beta_x^2}$. A similar expression is used for lines in the x-direction.

In practice, the direction of the lines is alternated, so that the method is efficient for grids with high aspect ratio cells in both directions. This implies that two multistage cycles are performed: in the first one, $Q^{(m+1)*}$ is computed with lines in one direction and in the second one with lines in the other direction.

The treatment of the turbulence equations is very similar. For these equations, there is no acoustic flux, nor artificial dissipation. The other fluxes are treated in the same way as the RANS fluxes. The source terms are treated partly explicitly and partly implicitly, based on the eigenvalues of the source term Jacobian (Merci *et al.*, 2000).

It is noteworthy that by expressing the discretized equations on the wedge-like control volume, no singularity problems occur on the symmetry axis ($y = 0$) : the equations are not solved for those grid points. Instead, symmetry boundary conditions are imposed: $\frac{\partial \phi}{\partial y} = 0$, where ϕ stands for any primitive variable but v. For that variable, the boundary condition on the axis is $v = 0$.

2.3 Treatment of higher order terms

In principle, the second order terms of the turbulent stress tensor (equation (6)) are treated explicitly (equation (30)). The justification is that the contribution of the second order terms of the stress tensor (equation (6)) to the global resulting force in the momentum equations is in general much smaller than the contribution of the first order terms and/or static pressure. However, in a stagnation region, the resulting force of the normal stress component perpendicular to a solid boundary is not negligible compared to the pressure force. Moreover, the second order part in expression (equation (6)) may have a contribution to the resulting force which is not negligible compared to the first order part. In such cases, explicit treatment is no longer possible.

Looking at the momentum equations, it is seen that the normal stress components have similar contributions as the effective pressure (e.g. equations (15), (18) and (30)). Consequently, these second order terms can easily be treated implicitly:

$$\tau_{yy}^{(2)^{(m+1)}*} = \frac{\tau_{yy}^{(2)^{(m)}}}{p_{\text{eff}}^{(m)}} p_{\text{eff}}^{(m+1)*}. \tag{37}$$

This is added to the acoustic flux in equation (30). Expression (37) is for a line in y-direction (as in equation (30)). A similar expression is used for a line in

x-direction. For the axisymmetric contribution (equation (22)), the same procedure is followed:

$$\tau_{zz}^{(2)^{(m+1)}*} = \frac{\tau_{zz}^{(2)^{(m)}}}{p_{\text{eff}}^{(m)}} p_{\text{eff}}^{(m+1)*}, \tag{38}$$

added to the acoustic flux (equation (17)) in equation (30). The second order part $\tau_{xy}^{(2)}$ can be treated explicitly, since its contribution to the force in the momentum equations is negligible compared to the first order part (which is treated implicitly, as seen in equation (30)). This has not only been observed for the test case in this paper, but also for all the test cases previously studied (Merci *et al.*, 2001). Note that implicit treatment of these terms would not be straightforward, since a numerically stable expression of the second order part of the shear stress components in terms of velocity derivatives is not easily done.

3. Description of the turbulence model

The eddy-viscosity in the first order part (equation (7)) is:

$$\mu_t = \rho f_\mu c_\mu k \tau_t, \tag{39}$$

with the damping function $f_\mu = 1.0 - \exp(-4.2 \times 10^{-2} \sqrt{R_y} - 5.1 \times 10^{-4} R_y^{1.5} - 3.65 \times 10^{-10} R_y^5)$ (with $R_y = \frac{\rho \sqrt{k} y}{\mu}$, where y is the normal distance from the nearest solid boundary), the turbulence time scale

$$\tau_t = \frac{k}{\varepsilon} + \sqrt{\frac{\mu}{\rho \varepsilon}}$$

and c_μ defined as:

$$c_\mu = \frac{1}{A_1 + A_s \eta + 15W} - {}^1\!/_2 \, c_1 \tau_t^2 (S_{mn} S_{nm} + \Omega_{mn} \Omega_{nm}), \tag{40}$$

with η defined as:

$$\eta = \tau_t \max(S, \Omega), \tag{41}$$

and the coefficient c_1 (Merci *et al.*, 2001):

$$\begin{cases} S \geq \Omega : c_1 = -600 f_W (A_1 + A_s \eta + 15W)^{-4} \\ S < \Omega : c_1 = -f_W \min(600(A_1 + A_s \eta + 15W)^{-4}; \\ 4 f_\mu (A_1 + A_s \eta + 15W)^{-1} / (\Omega^2 \tau_t^2 - S^2 \tau_t^2)) \end{cases} \tag{42}$$

The vorticity tensor is defined as:

$$\Omega_{ij} = \frac{1}{2}\left(\frac{\partial v_i}{\partial x_j} - \frac{\partial v_j}{\partial x_i}\right). \tag{43}$$

The tensor invariants are:

$$S = \sqrt{2S_{ij}S_{ij}}, \quad \Omega = \sqrt{2\Omega_{ij}\Omega_{ij}}. \tag{44}$$

The other parameters are $A_1 = 8$, $A_s = \sqrt{3}\cos\ \phi$ and

$$\phi = \frac{1}{3}\arccos(\sqrt{6}W),$$

with:

$$W = 2^{1.5}\frac{S_{ij}S_{jk}S_{ki}}{S^3}. \tag{45}$$

The term $15W$ in the denominator of equation (40) has been added to lower the value of the Nusselt number on the symmetry axis, as will be discussed later. The quantity W has the property that $W = 1/\sqrt{6}$ in axisymmetric impingement (or expansion) regions, while $W = 0$ for two-dimensional flows or in regions where shear is important. Therefore, addition of this term does not contaminate previous results in Merci *et al.* (2001).

In the expression for c_1, a factor f_W is introduced [compared to Merci *et al.* (2001)], to diminish the effect of the concave streamline curvature on turbulence in the stagnation region, which then results in better predictions for the heat transfer at the stagnation point, as will be discussed later. The function f_W is defined as:

$$f_W = 1 - 18W^2 + (72/\sqrt{6})W^3, \tag{46}$$

so that $f_W = 1$ when $W = 0$ and $f_W = 0$ when $W = 1/\sqrt{6}$ (and the derivatives with respect to W are zero at the edges of the domain of W).

The second order part of the turbulent stress tensor (equation (6)) is defined as:

$$\begin{aligned}\tau_{ij}^{(2)} = &- \rho k\tau_t^2 q_1\left(S_{ik}S_{kj} - {}^1/_3\delta_{ij}S_{lm}S_{ml}\right)\\ &- \rho k\tau_t^2(q_2 + q_1/6)(\Omega_{ik}S_{kj} - S_{ik}\Omega_{kj}),\end{aligned} \tag{47}$$

with the coefficients q_1 and q_2 (Merci *et al.*, 2001):

$$\begin{cases} q_1 = f_W(7 + 3\eta + 1.2 \times 10^{-2}\eta^3)^{-1} \\ q_2 = f_W(1.7 + 5.4\eta + 3 \times 10^{-2}\eta^3)^{-1} \end{cases} \quad (48)$$

where again f_W has been added to diminish the effect of the second order terms in the impingement region, resulting in better predictions at the stagnation point.

To conclude, it is remarked that equation (47) does not contain a quadratic term in the vorticity tensor: such terms must not be included (Speziale, 1998). In spite of this observation, the model of Craft *et al.* (2000) still contains such a term. It is also noted that in the original model (Merci *et al.*, 2001), there is a cubic term in the turbulent stress tensor, but since the flows under study are axisymmetric, this term is identically zero here and therefore omitted.

The steady-state transport equations for the turbulence quantities are:

$$\begin{cases} \frac{\partial}{\partial x_m}(\rho k v_m) = P_k - \rho\varepsilon + \frac{\partial}{\partial x_m}\left[\left(\mu + \frac{\mu_t}{\sigma_k}\right)\frac{\partial k}{\partial x_m}\right] \\ \frac{\partial}{\partial x_m}(\rho\varepsilon v_m) = \left(c_{\varepsilon 1}P_k - c_{\varepsilon 2}f_2\rho\varepsilon\right)\frac{1}{\tau_t} + \frac{\partial}{\partial x_m}\left[\left(\mu + \frac{\mu_t}{\sigma_\varepsilon}\right)\frac{\partial\varepsilon}{\partial x_m}\right] + E + Y_c. \end{cases} \quad (49)$$

with P_k the production of turbulent kinetic energy. The values $c_{\varepsilon 1} = 1.44$, $\sigma_k = 1$ and $\sigma_\varepsilon = 1.3$ are standard. The parameter $c_{\varepsilon 2}$ is (Merci *et al.*, 2001):

$$c_{\varepsilon 2} = 1.83 + \frac{0.075\Omega\tau_t}{1 + S^2\tau_t^2}, \quad (50)$$

with Ω given by equation (44). This ensures a correct transformation of the ε-equation for rotating reference frames when the absolute vorticity is used in equation (50) (Speziale, 1998). The damping function f_2 (Hanjalic and Launder, 1976) is $f_2 = 1 - 0.22\exp(-\mathrm{Re}_t^2/36)$, with $\mathrm{Re_t}$ the turbulence Reynolds number $\mathrm{Re_t} = \rho k\tau_t/\mu$. The low-Reynolds source term E is (Merci *et al.*, 2001):

$$E = -1.8(1 - f_\mu)\left(\mu + \frac{\mu_t}{\sigma_\varepsilon}\right)\frac{\partial k}{\partial x_m}\frac{\partial \tau_t^{-1}}{\partial x_m}. \quad (51)$$

It was found necessary, as in Craft *et al.* (2000), to add the "Yap correction" Y_c in the ε transport equation, in order to avoid overprediction of the heat transfer:

$$Y_c = 0.13\frac{k^2}{y^2}\max\left[\left(\frac{0.4k^{3/2}}{\varepsilon y} - 1\right);\ 0\right], \quad (52)$$

where (as in Craft *et al.*, 2000) implicitly the turbulent length scale has been defined as $l_t = k^{3/2}/\varepsilon$ and the equilibrium length scale as $l_e = 2.55y$, with y the normal distance from the nearest solid boundary.

As seen in equation (9), the linear gradient diffusion hypothesis is used for the turbulent heat flux q_t:

$$\bar{q}_t = -\frac{\mu_t c_p}{\mathrm{Pr}_t}\nabla T, \tag{53}$$

with Pr_t the turbulent Prandtl number. For the present model, $\mathrm{Pr}_t = 0.9$ is kept constant. Results will also be shown for a variable turbulent Prandtl number, determined from the formula of Kays and Crawford (1993):

$$\mathrm{Pr}_t = \left(0.5882 + 0.228\frac{\mu_t}{\mu} - 0.0441\left(\frac{\mu_t}{\mu}\right)^2\left[1 - \exp\left(-5.165\frac{\mu}{\mu_t}\right)\right]\right)^{-1}. \tag{54}$$

4. Application: turbulent impinging jets

4.1 Test case description

The geometry is shown in Figure 2. A fully developed turbulent flow through the nozzle is surrounded by a coflow. The nozzle exit, with diameter D, is at a distance H from the flat plate. The Reynolds number of the fully developed turbulent air flow in the nozzle exit, based on the diameter and the bulk velocity U_b, is $\mathrm{Re} = \frac{\rho U_b D}{\mu} = 23,000$.

The first extensive heat transfer measurements have been done by Baughn and Shimizu (1989), for different distances between the nozzle and the flat plate. Other sets of experimental data have been reported by Baughn *et al.* (1991), Yan (1993) and Lytle and Webb (1994). As mentioned in Behnia *et al.* (1999), there

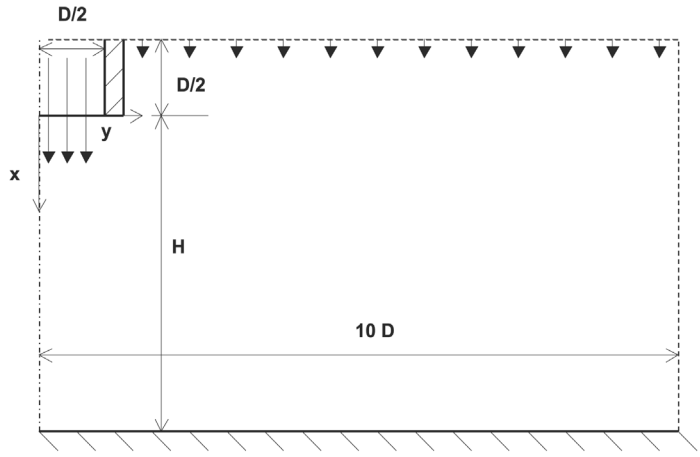

Figure 2.
Geometry and computational domain

are significant differences in the rates of heat transfer, despite the fact that most investigators reported uncertainties of the order of 5 per cent.

4.2 Computational grid and boundary conditions

The computational grid consists of 129×113 grid points. The domain starts $1/2D$ upstream of the nozzle exit, in order to correctly describe the entrainment of the coflow air. Radially, there are 40 cells within the pipe and four cells within the thickness of the pipe [equal to $0.0313D$ (Behnia *et al.*, 1999)]. Axially, there are 16 cells in the pipe. The grid is refined near the stagnation point (cells at the axis have size $\Delta y = 0.001D$). The four cells in the pipe thickness are equidistant. Radial stretching is applied from the axis outward and from the inner pipe radius inward, up to $r = D/4$. From the outer pipe radius to the upper boundary, stretching is applied, too. Axially, the cells between the inner and outer pipe radius are squares at the nozzle exit. At the stagnation point, the cell is square, too. Stretching is applied for all other cells.

At the inlet, a (separately calculated) fully developed turbulent pipe flow is imposed. Pressure is extrapolated from the flow field. The coflow air is a fully developed boundary layer (free stream velocity equal to 10 per cent of the mean pipe exit velocity; turbulence level equal to 1 per cent). The inlet profile for ε has been determined from fully developed conditions, with imposed fixed velocity and turbulence kinetic energy profiles (Merci *et al.*, 2002). Since the inlet of the computational domain is upstream of the nozzle exit, the entrainment is adequately described, even if the coflow inlet conditions are not very accurately imposed. The inlet temperature is prescribed as 293 K, whereas the temperature of the plate is prescribed as 313 K. All other boundary conditions are standard.

Note that in the experimental setup, a constant heat flux is imposed at the flat plate, rather than a constant temperature. However, as reported in Baughn and Shimizu (1989), results in terms of the Nusselt number, are independent of the (small) heat flux, so that imposing a constant temperature (which is numerically more feasible), is equivalent to imposing a constant heat flux. The temperature on the plate has been varied from 298 K to 318 K. The resulting profiles for the Nusselt number in equation (55) indeed do not change (not shown), illustrating that the results are independent from the exact value of the plate temperature (and the resulting heat flux). A test computation *a posteriori* with imposed heat flux indeed verified that the Nusselt number remains unchanged, compared to an imposed plate temperature.

4.3 Results

Results of the present model are compared to experimental data and to results from the low-Reynolds version of the standard k-ε model by Yang and Shih (1993). All results have been checked with respect to grid dependence by refining the computational grid to 257×225 points (not shown).

4.3.1 Heat transfer predictions. In Table I, the stagnation point value of the Nusselt number, is shown and is defined as:

$$\mathrm{Nu} = \frac{D\left|\frac{\partial(T_w - T_0)}{\partial x}\right|}{T_w - T_0}, \tag{55}$$

with T_w the plate surface temperature and T_0 the temperature at the pipe exit. The Yang and Shih (YS) model, with constant turbulent Prandtl number $\mathrm{Pr_t} = 0.9$, dramatically overpredicts Nu (first column). Note that the Nusselt number is identical to what is reported in Behnia *et al.* (1999), illustrating the accuracy of the presented numerical scheme.

Removing the work done by the viscous and turbulent stresses from the energy equation in equation (1), as well as the contributions from the kinetic energy (both mean and turbulent) in the total enthalpy (equation (8)), leads to the reduced energy, used in Behnia *et al.* (1999) and Craft *et al.* (2000). The second column of Table I (together with Figure 4) shows that this indeed does not affect the results. For all other results, the reduced energy equation is used.

Relating $\mathrm{Pr_t}$ to the eddy viscosity through equation (54), results in a practically negligible improvement (third column), as also reported in Behnia *et al.* (1998). The introduction of Y_c (equation (52)) into equation (49) on the other hand, does result in a serious improvement (fourth column), illustrating that the ε-equation is crucial for the stagnation point value of Nu. Also in the present model, Y_c is retained. The further improvement (fifth column) compared to the YS model with Y_c, stems from definition (40) of c_μ. In particular, the addition of the final term in the denominator of the first term lowers the value of c_μ, resulting in less overprediction of k and a better value for Nu.

The reason for this is seen in profiles at the symmetry axis (Figure 3). Picture "a" suggests practically identical mean velocity profiles for the different models. The reason is that pressure is the most important force (note that x is the distance from the plate in these figures). However, looking closer to the stagnation region (picture "b"), it is seen that the curves have a different behavior. In particular, the velocity is slightly higher with the present model for $x > 0.1D$ and lower for very small x. The reason is found in the momentum x-equation: $\frac{\partial \overline{u'u'}}{\partial x}$ is important near the stagnation point. Approaching the plate, $\overline{u'u'}$ increases (with a peak at $x \approx 0.1D$) and then decreases (picture "c"). The steeper the increase, the more rapidly the air is slowed down: the present model

Table I.
Nusselt number on the axis (red: reduced energy equation; vp: variable $\mathrm{Pr_t}$ (equation (54)); Yap: Y_c (equation (52)) added in equation (49))

Model	k-ε	k-ε (red)	k-ε (vp)	k-ε (Yap)	Present	Exp.
H/D = 2	311	312	302	183	152	135-150
H/D = 6	329	330	319	202	156	146-183

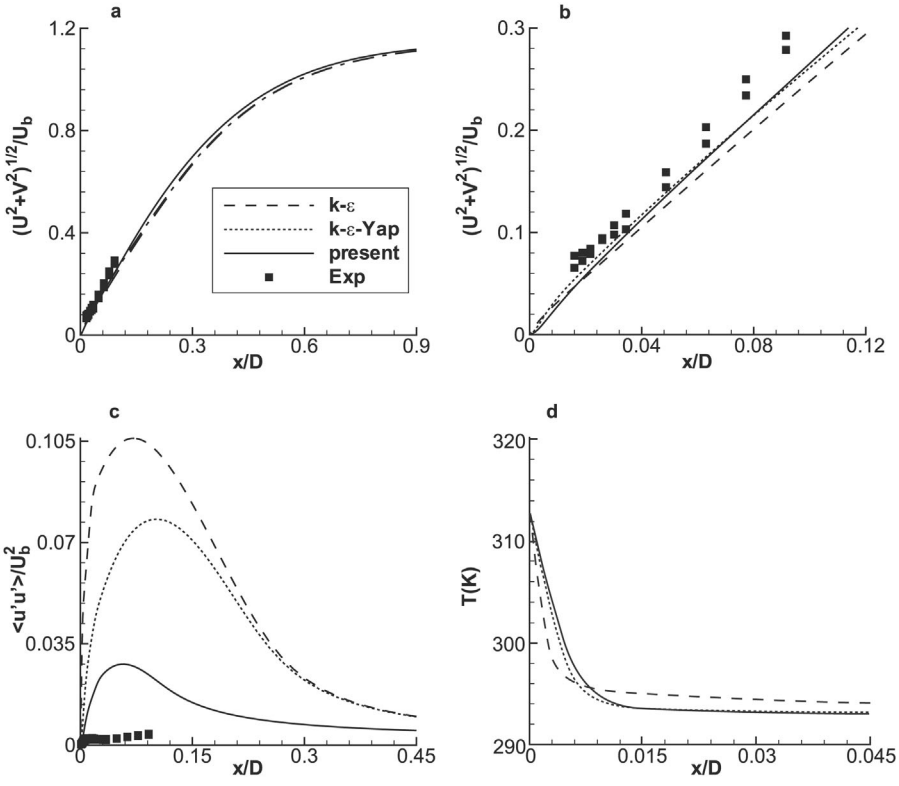

Figure 3.
Profiles on the symmetry axis for $H/D = 2$. (Note: x is the distance from the flat plate)

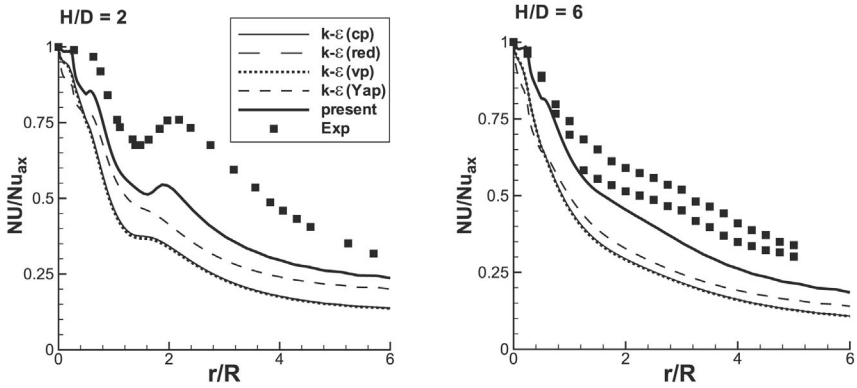

Figure 4.
Normalized local Nusselt number on the flat plate (legend: see Table I)

therefore has the highest velocity level for $x > 0.1D$. Similarly, a steeper decrease leads to a slower decrease in velocity (the pressure force is counteracted). This is reflected into a lower velocity for very small x with the present model. This affects the temperature profile on the axis (picture "d"): T is determined by the energy equation, which is a convection-diffusion equation. A higher (resp. lower) mean velocity means more convection (resp. diffusion). Picture "d" confirms this: the lower velocity for very small x gives rise to a less steep temperature increase near the plate. Through equation (55) this results in a lower (and more correct) stagnation point value for Nu. It is noteworthy here that the $\overline{u'u'}$ profile is not as good when f_W is not added in equations (48) and (42), leading to a higher value for Nu. The reasons are on the one hand that equation (48) (without f_W) increases $\overline{u'u'}$ for the same value of turbulence kinetic energy (and thus steepens the gradient), and on the other hand that equation (42) (without f_W) results in a global increase of k (and thus also $\overline{u'u'}$) in the stagnation region, due to the concave streamline curvature (Merci *et al.*, 2001). This complete reasoning is valid for both $H/D = 2$ and $H/D = 6$. To conclude, it is noted that $\overline{u'u'}$ is overpredicted near the stagnation point, but in itself this is not really of crucial importance: the derivative $\frac{\partial \overline{u'u'}}{\partial x}$ is much more important, since this is the quantity that contributes to the momentum x-equation.

Apart from the value at the stagnation point, the shape of the local Nusselt number profile along the plate (Figure 4) is also interesting. For both $H/D = 2$ and $H/D = 6$, the present model yields the best results. In particular, the increase in Nu around $r/R = 2$ for $H/D = 2$ is well reproduced. For $H/D = 6$ no such increase is observed in the experimental data, and indeed the model does not predict one, either. The YS model (with or without Y_c) is not able to reproduce the peak for $H/D = 2$. This illustrates an improvement of the shape of the profiles thanks to the non-linear constitutive law. Still, it must be admitted that there is a tendency towards under prediction of Nu. Possibly, a non-linear expression for the turbulent heat flux (instead of equation (53)) could resolve this. Finally, it is mentioned that using Pr_t from equation (54) indeed has a negligible influence on the shape of the Nusselt number profiles, so that, in combination with the very small effect on the value at the stagnation point (Table I), this does not seem a fruitful approach. Looking at the negligible influence at the shape of the Nusselt profiles (as already mentioned), it is justified to use the reduced energy equation.

To conclude, it is noted that good results are also obtained with the non-linear eddy viscosity model by Craft *et al.* (2000) and with the v^2-f model by (Behnia *et al.*, 1998 1999). The purpose of this paper is not to present a qualitatively superior model, as stated in the introduction. The advantages of the presented model are the absence of the quadratic vorticity term and the general applicability (which is no longer guaranteed in Craft *et al.* (2000), due to some "ad hoc" modifications) and the simplicity in use (in contrast to the v^2-f model, where extra equations need to be solved, compared to k-ε models).

4.3.2 Flow field predictions. In Figure 5, mean velocities are compared to measurements by Cooper *et al.* (1993). Measurements have been performed from $r = 0$ up to $r/D = 3$. The present model clearly gives the best results (except for $r/D = 3$, where the peak velocity is overpredicted. However, it is likely that the slope for larger x is better reproduced by the present model (as is the case for $r/D = 2.5$). Unfortunately, there are no experimental data to prove this.

Figure 6 shows the turbulent shear stress. Close to the stagnation line ($r/D = 0.5$) no model gives excellent results. The present model does give a lower value for the stress than the YS model. For all other radial positions, the present model clearly produces the best results: at $r/D = 1$ the stress is by far less overpredicted, while at the other positions the profiles are too wide for the YS model, while they are very well reproduced by the present model. This is mainly due to definition (equation (40)) of c_μ: introducing Y_c into equation (49) yields only a very small improvement here.

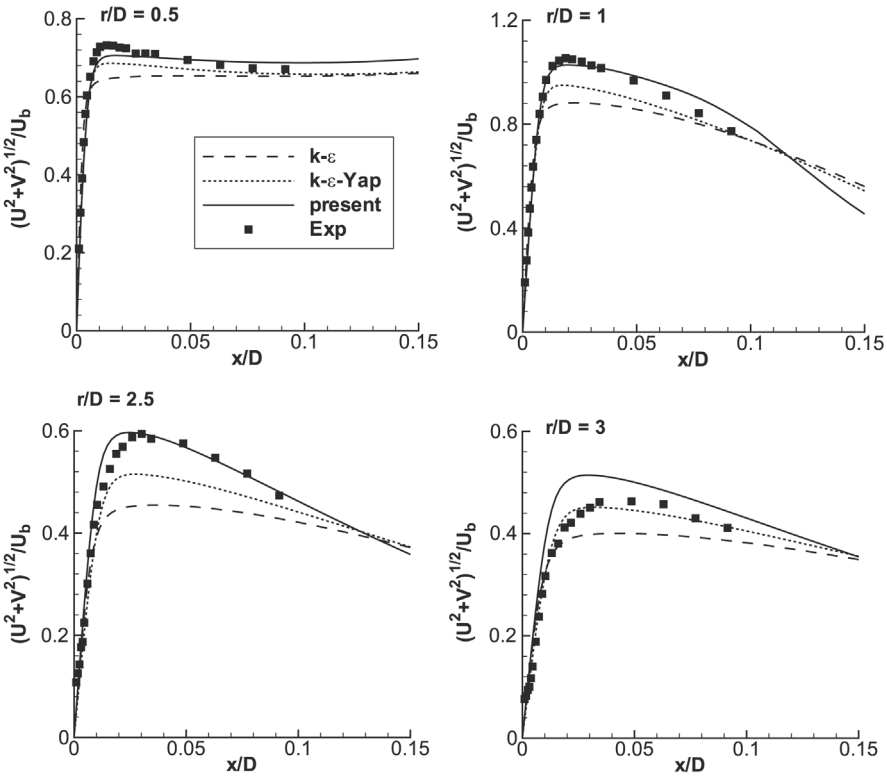

Figure 5.
Mean velocity profiles for $H/D = 2$. (Note: x is the distance from the flat plate)

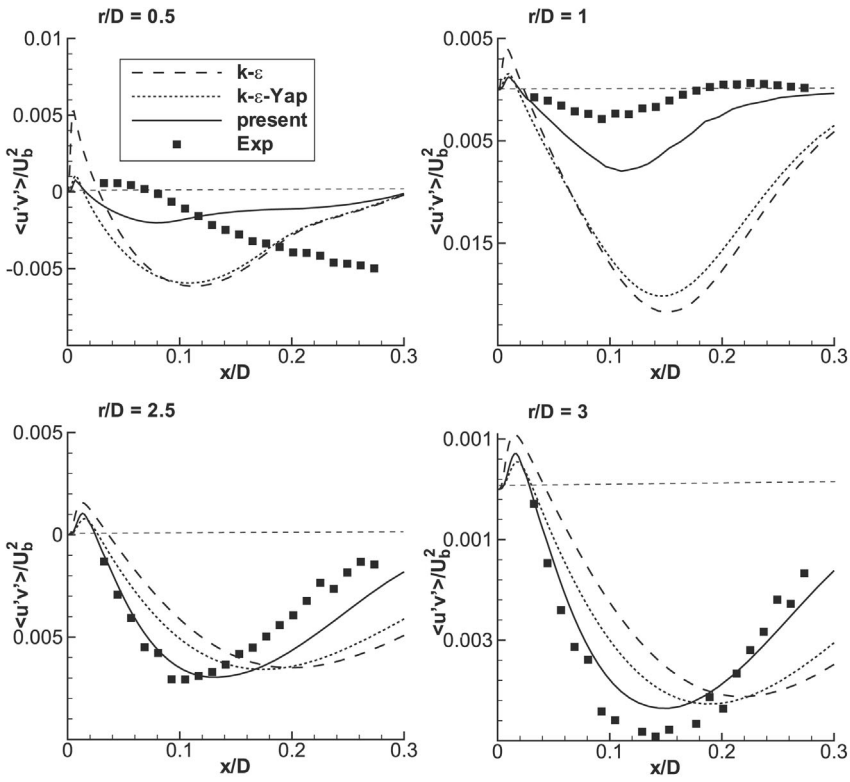

Figure 6.
Turbulent shear stress profiles for $H/D = 2$. (Note: x is the distance from the flat plate)

Also the normal turbulent stresses (Figures 7 and 8) are in much better agreement with the experimental data than the YS results. In Figure 7 it is seen that there is still a global overprediction. However, the overprediction is less severe for the present model than for the YS model, and the shape of the profiles (e.g. the peak positions for $r/D = 2.5$ and $r/D = 3$) is in good agreement with the experimental data. For $\overline{v'v'}$, similar observations are made (Figure 8). This stress component is very well reproduced by the present model for small r, while it is strongly overpredicted by the YS models. At the radial positions farther away from the axis, $\overline{v'v'}$ is under predicted by all models, but the under prediction is the least pronounced with the present model. Again, the shape of the profiles is also in better agreement with the experimental data than with the YS models.

The better predictions for the normal turbulent stresses are on the one hand due to the second order terms (47) in equation (6), which redistribute the turbulence kinetic energy to the different normal stresses. At least equally important is the fact that the value of k is much better predicted with the present model (in particular in the stagnation region), again thanks to the

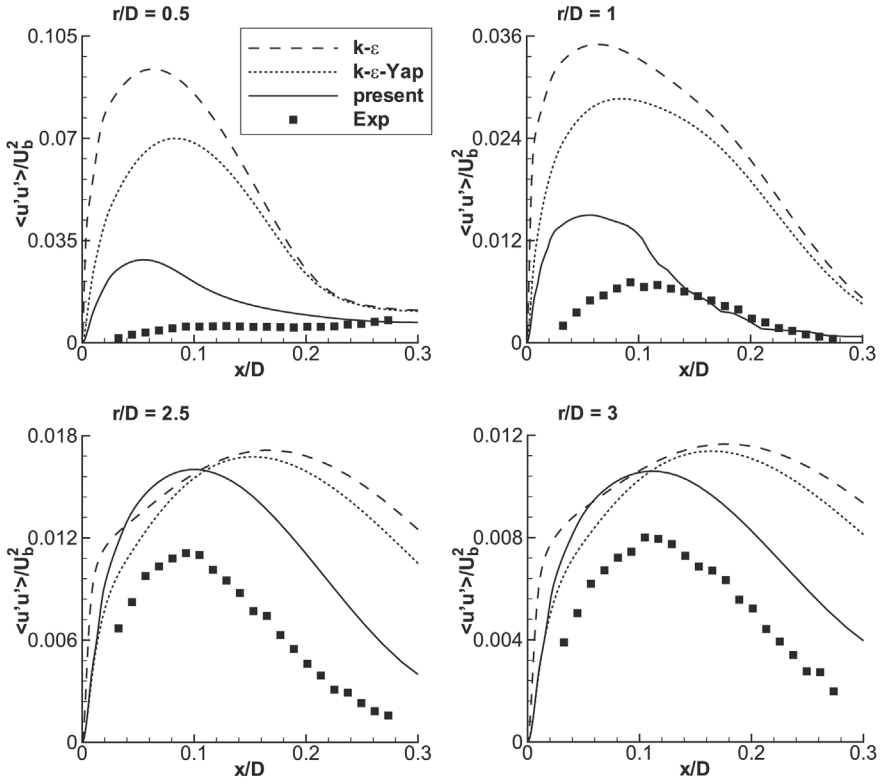

Figure 7.
Profiles of $\overline{u'u'}$ for $H/D = 2$. (Note: x is the distance from the flat plate)

definition of c_μ: addition of Y_c to equation (49) is not sufficient to obtain accurate results.

Conclusions

An efficient, robust and accurate numerical method for two-dimensional laminar flows, has been extended for the calculation of heat transfer in an axisymmetric turbulent jet, impinging onto a heated flat plate.

Some well-known features of the standard k-ε model are correctly reproduced by the presented numerical scheme: the excessive stagnation point value for the Nusselt number is identical to the one reported in Behnia *et al.* (1999) and the use of a variable turbulent Pr number hardly affects the results. It was also illustrated that the energy equation can be simplified by neglecting the work done by the viscous and turbulent stresses, and the kinetic energy contribution in the total enthalpy, without affecting the results.

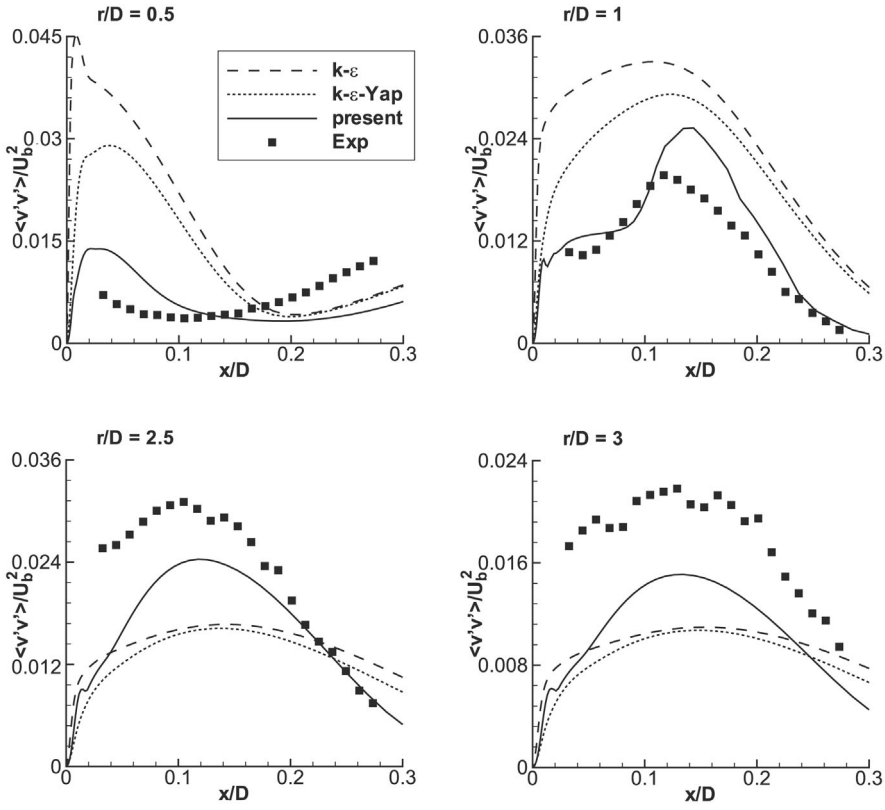

Figure 8.
Profiles of $\overline{v'v'}$ for $H/D = 2$. (Note: x is the distance from the flat plate)

A non-linear eddy viscosity model has been presented, with the Yap correction added to the ε transport equation. It was illustrated that, for numerical stability, the higher order terms in the expression for the normal turbulent stresses must be treated implicitly.

The results with the non-linear eddy viscosity are in good agreement with experimental data. For the heat transfer predictions, both the stagnation point value of the Nusselt and the shape of the local Nu profiles along the plate are well predicted for different distances between the nozzle and the plate, although there is a tendency towards under prediction.

The mean velocity profiles are in good agreement with the experimental data. They are more accurate than what is obtained with the standard k-ε model. For the turbulent stresses (both the shear stress and the normal stress components), this is a fortiori true. Both the dissipation rate transport equation and the higher order expression for the turbulent stress tensor (and in particular the definition of c_μ) have a contribution to the improvements of the results.

References

Baughn, J.W. and Shimizu, S. (1989), "Heat transfer measurements from a surface with uniform heat flux and an impinging jet", *Journal of Heat Transfer*, Vol. 111, pp. 1096-8.

Baughn, J.W., Hechanova, A. and Yan, X. (1991), "An experimental study of entrainment effects on the heat transfer from a flat surface to a heated circular impinging jet", *Journal of Heat Transfer*, Vol. 113, pp. 1023-5.

Behnia, M., Parneix, S. and Durbin, P.A. (1998), "Prediction of heat transfer in an axisymmetric turbulent jet impinging on a flat plate", *International Journal of Heat and Mass Transfer*, Vol. 41 No. 12, pp. 1845-55.

Behnia, M., Parneix, S., Shabany, Y. and Durbin, P.A. (1999), "Numerical study of turbulent heat transfer in confined and unconfined impinging jets", *International Journal of Heat and Fluid Flow*, Vol. 20, pp. 1-9.

Cooper, D., Jackson, D.C., Launder, B.E. and Liao, G.X. (1993), "Impinging jet studies for turbulence model assessment - I. Flow field experiments", *International Journal of Heat and Mass Transfer*, Vol. 36 No. 10, pp. 2675-84.

Craft, T.J., Iacovides, H. and Yoon, J.H. (2000), "Progress in the use of non-linear two-equation models in the computation of convective heat-transfer in impinging and separated flows", *Flow, Turbulence and Combustion*, Vol. 63, pp. 59-80.

Durbin, P. (1991), "Near-wall turbulence closure without damping functions", *Theoretical and Computational Fluid Dynamics*, Vol. 3, pp. 1-13.

Hanjalic, K. and Launder, B.E. (1976), "Contribution towards a Reynolds-stress closure for low-Reynolds-number turbulence", *Journal of Fluid Mechanics*, Vol. 74 No. 4, pp. 593-610.

Kays, W.M. and Crawford, M.E. (1993), *Convective Heat and Mass Transfer*, 3rd ed., McGraw-Hill.

Lytle, D. and Webb, B. (1994), "Air jet impingement heat transfer at low nozzle-plate spaces", *International Journal of Heat and Mass Transfer*, Vol. 37, pp. 1687-97.

Merci, B., Steelant, J., Vierendeels, J., Riemslagh, K. and Dick, E. (2000), "Computational treatment of source terms in two-equation turbulence models", *AIAA Journal*, Vol. 38 No. 11, pp. 2085-93.

Merci, B., De Langhe, C., Vierendeels, J. and Dick, E. (2001), "A quasi-realizable cubic low-Reynolds eddy-viscosity turbulence model with a new dissipation rate equation", *Flow, Turbulence and Combustion*, Vol. 66 No. 2, pp. 133-57.

Merci, B., Dick, E., Vierendeels, J. and De Langhe, C. (2002), "Determination of ε at inlet boundaries", *International Journal of Numerical Methods for Heat and Fluid Flow*, Vol. 12 No. 1, pp. 65-80.

Speziale, C.G. (1998), "A consistency condition for non-linear algebraic Reynolds stress models in turbulence", *International Journal of Non-Linear Mechanics*, Vol. 33 No. 4, pp. 579-84.

van Leer, B. (1977), "Toward the ultimate conservative difference scheme III. Upstream-centered finite-difference schemes for ideal compressible flow", *Journal of Computational Physics*, Vol. 23, pp. 263-75.

Vierendeels, J., Riemslagh, K. and Dick, E. (1999), "A multigrid semi-implicit line-method for viscous incompressible and low-Mach-number flows on high aspect ratio grids", *Journal of Computational Physics*, Vol. 154, pp. 310-41.

Vierendeels, J., Merci, B. and Dick, E. (2001), "Numerical study of natural convective heat transfer with large temperature differences", *International Journal of Numerical Methods for Heat and Fluid Flow*, Vol. 11 No. 4, pp. 329-41.

Weiss, J. and Smith, W. (1995), "Preconditioning applied to variable and constant density flows", *AIAA Journal*, Vol. 33 No. 11, pp. 2050-7.

Yan, X.(1993), "A preheated-wall transient method using liquid crystals for the measurement of heat transfer on external surfaces and in ducts", PhD thesis, University of California, Davis.

Yang, Z.Y. and Shih, T.H. (1993), "A new time scale based k-ε model for near-wall turbulence", *AIAA Journal*, Vol. 31 No. 7, pp. 1191-8.

Yap, C.R. (1987), "Turbulent heat and momentum transfer in recirculating and impinging flows", PhD thesis, Faculty of Technology, University of Manchester.